Double-ionization mechanisms and asymmetry parameters for $(e,3e-1e)$ reactions

J. Berakdar
Atomic and Molecular Physics Laboratories, Research School of Physical Sciences and Engineering, Australian National University, Canberra, Australian Capital Territory 0200, Australia
(Received 10 October 1995)

In this work the cross section for the coincident detection of two electrons following double ionization of helium by fast electrons is analyzed. Structures arising in cross sections are associated with ionization mechanisms. The role of electronic correlations is elucidated. The theory is compared with available experimental data and suggestions for future experiments are made where results can be analyzed in terms of generalized asymmetry parameters and directly linked with well studied asymmetry parameters for double photoionization. Further, a method of calibrating relative $(e,3e-1e)$ cross sections to double photoionization cross sections is proposed.

PACS number(s): 34.80.Ht, 34.80.Dp

I. INTRODUCTION

Recent advances in coincidence detection technique have rendered possible the measurement of fully differential double-ionization cross sections of atoms by fast electron impact. These so-called $(e,3e)$ experiments have been performed using argon and krypton targets [1–3]. The projectile electrons suffer only very small momentum loss during the collisions. The major aim of these studies is to investigate electronic correlations in initial and final channels. In principle, the $(e,3e)$ technique can also be used to obtain an estimate of the electron-momentum profile in the initial state. Under the above described kinematical condition the $(e,3e)$ process is closely related to double ionization by one linearly polarized photon (DPI) [4–7] and electronic correlations can be equivalently studied by DPI methods. The $(e,3e)$ technique, however, offers a different approach to electronic correlations by assigning collisional ionization mechanisms to structures arising in the cross section (see Ref. [8] and below). This gives a clear visual picture of the fragmentation process.

The fully differential cross section of the $(e,3e)$ process is obtained by an energy- and angle-resolved detection of the two ionized electrons in coincidence with deflected projectile. For helium only the solid angle of the scattered projectile has then to be resolved. Such measurements are unfortunately hampered by low counting rates so that only some specific atomic targets are experimentally accessible at present. In particular, such experiments are not yet feasible for the helium target, which constitutes the simplest case of such reactions. Thus, one has to resort to the less technically elaborate case, the so-called $(e,3e-1e)$ reaction, where only two of the three electrons present in the final state are detected in coincidence [9–11]. It is the aim of this work to analyze possible arrangements and outcomes of an $(e,3e-1e)$ experiment. Details of $(e,3e)$ cross sections have been investigated by numerous theoretical models [12–17,8]. Since three electrons are present in the final channel different types of experimental arrangements for $(e,3e-1e)$ experiments are possible. For example, one could perform an energy- and angle-resolved detection of the two ejected electrons and integrate over the scattered projectile. Such cross sections are most suitable to analyze electronic correlations and collisional ionization mechanisms. However, the analogy to DPI cross sections is lost, since integration over the scattered electron implicates an integration over the momentum-transfer vector, which usually corresponds to the polarization vector in DPI experiments. This kind of $(e,3e-1e)$ experiments is addressed in Sec. III after a brief introduction to the theoretical model. To restore the connection to DPI reactions the momentum-transfer vector has to be fixed. This can be achieved by integrating over one secondary electron and determining the momenta of the other ionized electron and the scattered projectile, simultaneously. In this case the cross section of $(e,3e-1e)$ reactions can be calibrated to DPI data and analyzed in terms of generalized asymmetry parameters that connect to well known asymmetry parameters of DPI reactions. In addition, as shown in Sec. IV, this case is appropriate to systematically study the optical limit as well as electronic correlations. The results of this work can also be generalized to the case of double ionization by arbitrary, structureless charged projectiles using the scaling formula presented previously [17]. Atomic units are used throughout.

II. THEORETICAL CONSIDERATION

We consider the double ionization of the helium atom in its singlet ground state by a fast electron with momentum $\mathbf{k}_i$ (fast with respect to the Bohr velocity of the bound electrons). Further, we assume little momentum being transferred from the projectile to the target atom so that a Born-type approximation in the projectile-target potential can be employed [18–20]. The z axis is defined by the direction $\mathbf{k}_i$. Assuming the nucleus to be infinitely heavy compared with the electron mass, the multiple differential cross section for the two atomic electrons "a" and "b" being ejected into directions $d\Omega_a$ and $d\Omega_b$ with energies E_a and E_b and for the projectile being scattered into the solid angle $d\Omega_0$ is given by

$$\frac{d^8\sigma}{d\Omega_a d\Omega_b d\Omega_0 dE_a dE_b} = (2\pi)^4 \frac{k_a k_b k_0}{k_i} |T_{fi}|^2 \quad . \qquad (1)$$

The momenta of the ionized electrons are given by $k_a=\sqrt{2E_a}$, $k_b=\sqrt{2E_b}$, whereas the momentum of the projectile electron in the final channel is labeled by k_0. The two-particle transition matrix element T_{fi} can be expressed as the sum of three terms,

$$T_{fi}=T_T+T_a+T_b. \tag{2}$$

The transition amplitudes T_T, T_a, T_b describe direct scattering off the nucleus, electron a, and electron b, respectively, i.e.,

$$T_T=\left\langle \psi^-_{\mathbf{k}_a,\mathbf{k}_b}(\mathbf{r}_a,\mathbf{r}_b),\mathbf{k}_i\left|\frac{-2}{r_0}\right|\ \varphi(\mathbf{r}_a,\mathbf{r}_b),\mathbf{k}_0\right\rangle$$

$$=\frac{4\pi}{q^2}\langle\psi^-_{\mathbf{k}_a,\mathbf{k}_b}(\mathbf{r}_a,\mathbf{r}_b)|2|\varphi(\mathbf{r}_a,\mathbf{r}_b)\rangle, \tag{3}$$

$$T_a=\left\langle \psi^-_{\mathbf{k}_a,\mathbf{k}_b}(\mathbf{r}_a,\mathbf{r}_b),\mathbf{k}_i\left|\frac{1}{|\mathbf{r}_a-\mathbf{r}_0|}\right|\varphi(\mathbf{r}_a,\mathbf{r}_b),\mathbf{k}_0\right\rangle$$

$$=-\frac{4\pi}{q^2}\langle\psi^-_{\mathbf{k}_a,\mathbf{k}_b}(\mathbf{r}_a,\mathbf{r}_b)|\exp(i\mathbf{q}\cdot\mathbf{r}_a)|\varphi(\mathbf{r}_a,\mathbf{r}_b)\rangle, \tag{4}$$

$$T_b=\left\langle \psi^-_{\mathbf{k}_a,\mathbf{k}_b}(\mathbf{r}_a,\mathbf{r}_b),\mathbf{k}_i\left|\frac{1}{|\mathbf{r}_b-\mathbf{r}_0|}\right|\varphi(\mathbf{r}_a,\mathbf{r}_b),\mathbf{k}_0\right\rangle$$

$$=-\frac{4\pi}{q^2}\langle\psi^-_{\mathbf{k}_a,\mathbf{k}_b}(\mathbf{r}_a,\mathbf{r}_b)|\exp(i\mathbf{q}\cdot\mathbf{r}_b)|\varphi(\mathbf{r}_a,\mathbf{r}_b)\rangle. \tag{5}$$

In Eqs. (3)–(5) the momentum-transfer vector $\mathbf{q}=\mathbf{k}_i-\mathbf{k}_0$ has been introduced. The vectors $\mathbf{r}_a,\mathbf{r}_b,\mathbf{r}_0$ refer respectively to the positions of the two target electrons and the projectile with respect to the nucleus. The two-electron bound-state wave function of He($^1S^e$) is denoted by $\varphi(\mathbf{r}_a,\mathbf{r}_b)$, whereas the wave function $\psi^-_{\mathbf{k}_a,\mathbf{k}_b}(\mathbf{r}_a,\mathbf{r}_b)$ describes two outgoing electrons in the double continuum of the He^{2+} atom. Within an exact treatment of the motion of the two secondary electrons the scattering amplitude T_T, given by Eq. (3), vanishes identically, since the wave functions $\psi^-_{\mathbf{k}_a,\mathbf{k}_b}(\mathbf{r}_a,\mathbf{r}_b)$ and $\varphi(\mathbf{r}_a,\mathbf{r}_b)$ are then eigenfunctions of the same Hamiltonian for different eigenvalues. The exact forms of these wave functions are, however, not known and the overlap of approximate expressions for $\psi^-_{\mathbf{k}_a,\mathbf{k}_b}(\mathbf{r}_a,\mathbf{r}_b)$ and $\varphi(\mathbf{r}_a,\mathbf{r}_b)$ is, in general, finite. Nevertheless, approximate initial- and final-state wave functions can be orthogonalized by defining a final-state wave function as

$$\bar{\psi}^-_{\mathbf{k}_a,\mathbf{k}_b}(\mathbf{r}_a,\mathbf{r}_b)=\psi^-_{\mathbf{k}_a,\mathbf{k}_b}(\mathbf{r}_a,\mathbf{r}_b)-\frac{T_T^*}{2}\varphi(\mathbf{r}_a,\mathbf{r}_b). \tag{6}$$

Thus, the term T_T, as given by Eq. (3), vanishes when using the wave function $\bar{\psi}^-_{\mathbf{k}_a,\mathbf{k}_b}(\mathbf{r}_a,\mathbf{r}_b)$ to describe the final state of the secondary electrons. Note, however, that the nonphysical overlap $\langle\psi^-_{\mathbf{k}_a,\mathbf{k}_b}(\mathbf{r}_a,\mathbf{r}_b)|\varphi(\mathbf{r}_a,\mathbf{r}_b)\rangle$ still enters in the wave function [Eq. (6)]. Results obtained using orthogonalized and nonorthogonalized final-state wave functions are, in general, different and *a priori* it is not obvious which wave function is the better approximation. Nevertheless, for declining momentum transfer, results of orthogonalized and nonorthogonalized wave functions converge to the same limit. For small momentum transfer q the exponentials in Eqs. (4,5) can be expanded with respect to q leading to the optical relation

$$T_{fi}=-iq\langle\psi^-_{\mathbf{k}_a,\mathbf{k}_b}(\mathbf{r}_a,\mathbf{r}_b)|\hat{\mathbf{q}}(\mathbf{r}_a+\mathbf{r}_b)|\varphi(\mathbf{r}_a,\mathbf{r}_b)\rangle+O(q^2). \tag{7}$$

From (7) it is clear that, to the first order in q, the $(e,3e)$ cross section is closely related to cross sections of double photoionization by linearly polarized light in length formulation. The electric vector is pointing into the $\mathbf{q}$ direction. In the optical limit initial and final states are always orthogonal because only the odd parity part of the final-state contributes to the matrix element, and this odd-parity final state is automatically orthogonal to the even initial state. The energy balance can be expressed as

$$E_i-\epsilon=E_0+E_a+E_b. \tag{8}$$

In Eq. (8) the energies of the projectile electron in the initial and final channels are designated by E_i and E_0, respectively. Further, the energy of the recoiling nucleus has been neglected due to the massive nuclear mass. The positive binding energy of the target electrons is denoted by $\epsilon\approx 2.9037$ a.u. The translational invariance of the whole experiment leads to the conservation law of the linear momentum

$$\mathbf{q}=\mathbf{k}_a+\mathbf{k}_b+\mathbf{k}_{ion}, \tag{9}$$

where $\mathbf{k}_{ion}$ is the recoil momentum of the nucleus that is assumed to be initially at rest.

III. $(e,3e-1e)$ REACTIONS

Due to the presence of three electrons in the final channel an $(e,3e-1e)$ experiment can be carried out in different ways. At first we consider the case where the two secondary electrons are angle- and energy-resolved in coincidence with the ion-charge state, i.e., the scattered electron is not detected:

$$\sigma_{a,b}:=\frac{d^6\sigma}{d\Omega_a d\Omega_b dE_a dE_b}$$

$$=\int\frac{d^8\sigma}{d\Omega_a d\Omega_b d\Omega_0 dE_a dE_b}d\Omega_0. \tag{10}$$

Cross sections obtained according to Eq. (10) are suitable to analyze ionization mechanisms and electronic correlations, as we will see below. However, these cross sections cannot be related to fully differential DPI cross sections, e.g., as given by Refs. [4–7], since the integration involved in Eq. (10) runs essentially over the momentum-transfer vector $\mathbf{q}$ in some limited interval. This would correspond to integration over polarization vectors in DPI experiments [compare Eq. (7)]. Such DPI data are not available. $(e,3e-1e)$ cross sections that compare with existing DPI data will be investigated in the next section. To analyze the structure of $\sigma_{a,b}$ we employ for the wave function $\psi^-_{\mathbf{k}_a,\mathbf{k}_b}(\mathbf{r}_a,\mathbf{r}_b)$ of the two slow escaping electrons the same symmetric approximate expression, and its orthogonalized form, as used in a previous work [8]:

$$\psi^{-}_{\mathbf{k}_a,\mathbf{k}_b}(\mathbf{r}_a,\mathbf{r}_b)\approx(2\pi)^{-3}N\ \exp(i\mathbf{k}_a\cdot\mathbf{r}_a+i\mathbf{k}_b\cdot\mathbf{r}_b)_1F_1(i\alpha_{ab},1,-i[k_{ab}r_{ab}+\mathbf{k}_{ab}\cdot\mathbf{r}_{ab}])_1F_1(i\alpha_{Ta},1,-i[k_ar_a+\mathbf{k}_a\cdot\mathbf{r}_a])_1F_1(i\alpha_{Tb},1,-i[k_br_b+\mathbf{k}_b\cdot\mathbf{r}_b]) \tag{11}$$

with the normalization factor

$$N=\exp(-\pi\alpha_{ab}/2)\Gamma(1-i\alpha_{ab})\exp(-\pi\alpha_{Ta}/2)\times\Gamma(1-i\alpha_{Ta})\exp(-\pi\alpha_{Tb}/2)\Gamma(1-i\alpha_{Tb}).$$

Here $\mathbf{k}_{ab}$ is the momentum conjugate to the interelectronic coordinate $\mathbf{r}_{ab}=\mathbf{r}_b-\mathbf{r}_a$. The Sommerfeld parameters are defined as

$$\alpha_{ab}=\frac{1}{2k_{ab}},\qquad \alpha_{Ta}=\frac{-2}{k_a},\qquad \alpha_{Tb}=\frac{-2}{k_b}. \tag{12}$$

The singlet ground state of helium is described by a Hylleraas-type wave function that contains radial and angular correlations [21], i.e.,

$$\varphi(\mathbf{r}_a,\mathbf{r}_b)\approx N\{\exp[-C_ar_a-C_br_b]+\exp[-C_br_a-C_ar_b]\}\exp[C_{ab}|\mathbf{r}_a-\mathbf{r}_b|], \tag{13}$$

where N is normalization factor and C_a, C_b, and C_{ab} are positive real numbers used to minimize the binding energy of He($^1S^e$). As a prototype we examine the experimentally investigated collision geometry [11] in which the incident energy is fixed to $E_i=5525$ eV and one electron, say electron a, is detected at a fixed angle perpendicular to the incident direction. The energy transferred to the target is fixed to $E_a+E_b=35$ eV. Further, coplanar geometry is chosen in which case $\mathbf{k}_i,\mathbf{k}_a$ and $\mathbf{k}_b$ are linearly dependent. The angular distribution of electron b has three limiting cases, namely, $E_b\gg E_a, E_b=E_a$ or $E_a\gg E_b$. Basically, in all cases a maximum in the cross section $\sigma_{a,b}$ is expected whenever the Bethe sphere, as defined previously [8], is approached, i.e., when the energy and momentum transferred to the target are directly absorbed by the ionized electrons. As we integrate over $\mathbf{q}$ to obtain $\sigma_{a,b}$ [Eq. (10)] the Bethe sphere conditions [8] are not directly applicable. However, the integrated quantity

$$k_{av}(\Omega_a,\Omega_b,E_a,E_b)=\int k_{ion}(\Omega_o,\Omega_a,\Omega_b,E_a,E_b)d\Omega_o \tag{14}$$

is well defined and indicates the average momentum transferred to the nucleus at certain geometry. Thus, a minimum in $k_{av}(\Omega_b)$ corresponds to a maximum in the angular distribution $\sigma_{a,b}(\Omega_b)$. This is demonstrated in Fig. 1(a), where $E_b=34.8$ eV$\gg E_a=0.2$ eV. The minimum of k_{av} as function of $\theta_b:=\cos^{-1}\hat{\mathbf{k}}_i\cdot\hat{\mathbf{k}}_b$ is located at $\theta_b\approx64°$. Correspondingly, the direct scattering off electron b that provides the main contribution to $\sigma_{a,b}(\theta_b)$ peaks at $\theta_b\approx70°$ [see Fig. 1(b)]. This means, predominantly, that the projectile electron directly hits electron b, which escapes carrying away almost the whole momentum transferred to the target. Electron a is then shaken loose by the sudden change in the effective nuclear charge. Hence, the direct projectile scattering off electron a is almost structureless and yields a minor contribution to the binary peak located at $\theta_b\approx70°$ [compare Fig. 1(b)]. This double-ionization mechanism, as explicitly demonstrated here, has been previously predicted in Ref. [3]. Clearly, for He this mechanism depends strongly on the description of the initial state, which decides the amount of shake-off [22,23] and is less sensitive to the electronic correlations in the final state [8]. The actual shape of $\sigma_{a,b}(\theta_b)$ is determined by the coherent sum of the amplitudes T_a and T_b, as given by Eq. (2). The interference of these amplitudes is still remarkably strong due to the relatively small energy separation E_b-E_a. The case $E_a\gg E_b$ yields similar results [24] with the interpretation as above, except that the roles of electron a and electron b are interchanged. It is important to

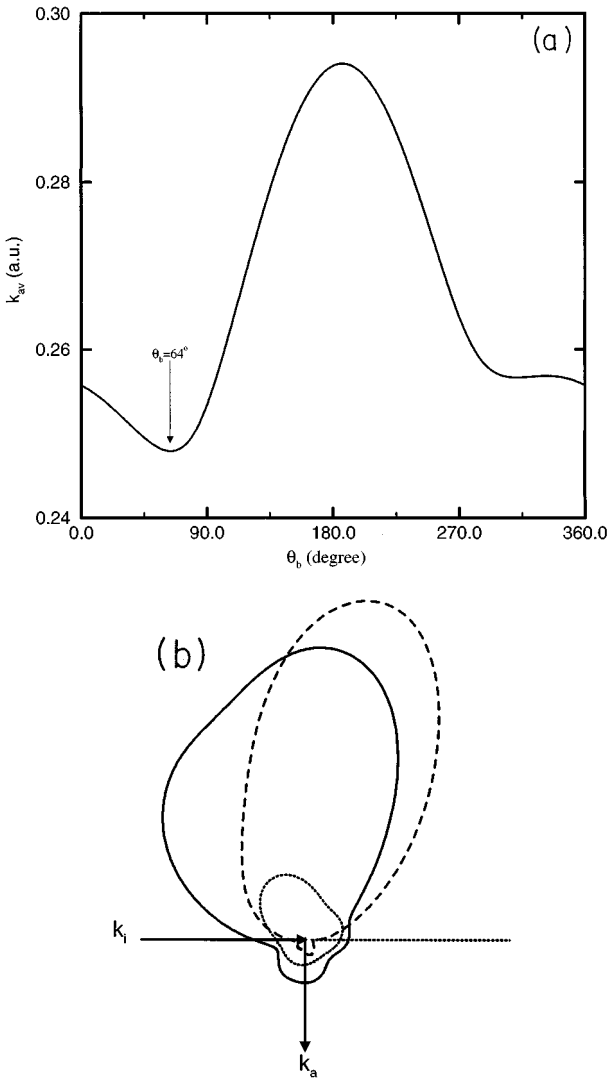

FIG. 1. (a) Average momentum transferred to the nucleus k_{av} as a function of $\theta_b=\cos^{-1}\hat{\mathbf{k}}_i\cdot\hat{\mathbf{k}}_b$. The collision geometry is chosen to be $E_i=5525$ eV, $E_a+E_b=35$ eV, $E_a=0.2$ eV, $\mathbf{k}_i\cdot\mathbf{k}_a=0$, and $(\mathbf{k}_i\times\mathbf{k}_a)\cdot\mathbf{k}_b=0$. (b) Angular distribution $\sigma_{a,b}(\theta_b)$ with respect to $\hat{\mathbf{k}}_i$ [see Eq. (10)]. The collision geometry is the same as in (a). An orthogonal final-state wave function has been employed. The incoherent contributions of T_b, i.e., $T_{fi}=T_b$ (dashed curve) and of T_a, i.e., $T_{fi}=T_a$ (dotted), are shown along with their coherent sum (solid curve).

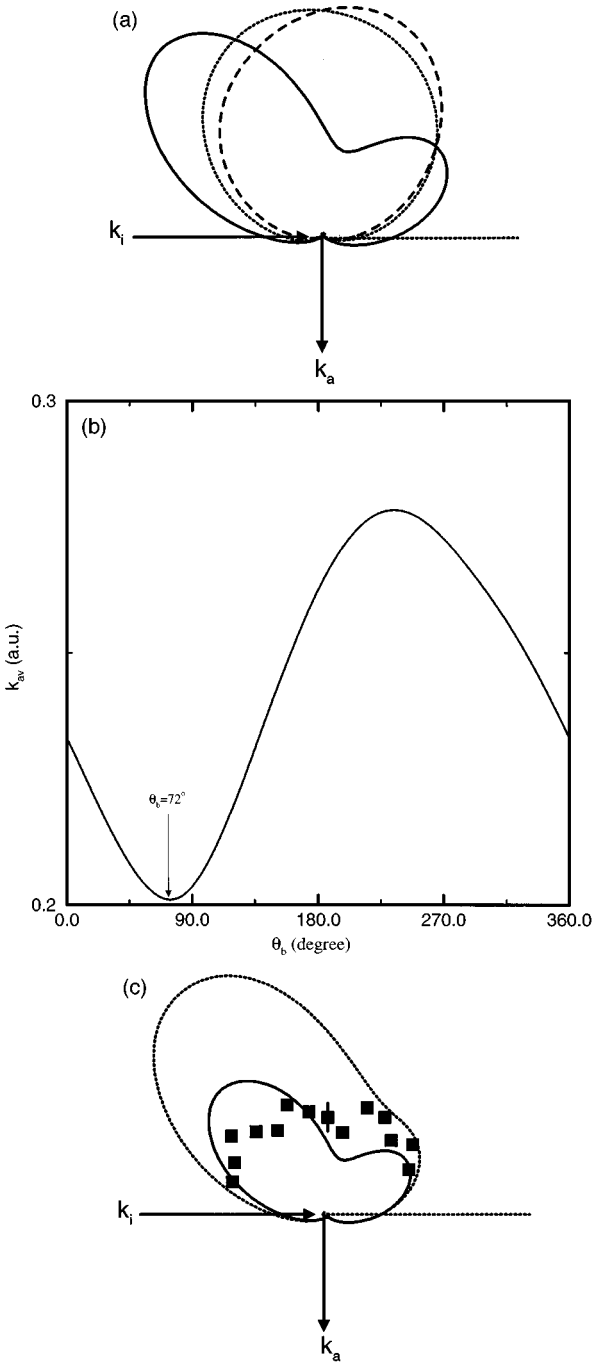

FIG. 2. (a) Same collision geometry as in Fig. 1(b); however, $E_a=E_b$. Wave functions and curves are also the same as in Fig. 1(b). (b) The angular distribution of the average momentum k_{av} for the case depicted in (a). (c) The same collision arrangement as in (a). Results of orthogonalized (solid curve) and nonorthogonalized (dotted curve) wave functions are displayed. Experimental data (squares) have been provided by Ref. [11]. The relative experimental data have been normalized to theory at $\hat{\mathbf{k}}_i\cdot\hat{\mathbf{k}}_b=\cos(\pi/6)$. The magnitude of the cross section calculated with the nonorthogonalized form is equal to 1.75×10^{-5} a.u. at $\hat{\mathbf{k}}_i\cdot\hat{\mathbf{k}}_b=\cos(\pi/2)$.

notice here that k_{av} does not vanish even on the Bethe sphere. This is due to the fact that the momentum conservation law [Eq. (9)] is the result of a translational invariance of the system and does not account for internal degrees of freedom of the target initially at rest. The momentum distribution of the nucleus in the initial bound state is exactly cancelled to a zero linear momentum by the presence of the bound electrons. When the electrons are directly ionized and no momentum is transferred to the nucleus during the collision the nucleus recoils with a momentum equal to the initial binding momenta of the electrons before the collision. This fact can be used to actually image the momentum distribution of the bound electrons (Compton profile), as done in an analogous way in $(e,2e)$ experiments [25].

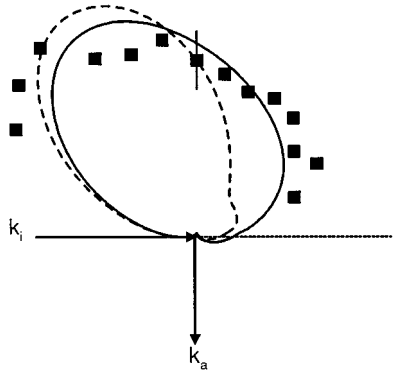

FIG. 3. Angular distribution $\sigma_{a,b}(\theta_b)$ in the case $E_a=7$ eV for $(e,3e-1e)$ on He(^1S). The experimental setup is the same as in Fig. 2(a). Calculations using orthogonalized (solid curve) and nonorthogonalized (dotted curve) wave functions are depicted along with experimental data (squares) [11]. Experimental data are relative. The magnitude of the cross section calculated with the nonorthogonalized form is equal to 2.573×10^{-4} a.u. at $\hat{\mathbf{k}}_i\cdot\hat{\mathbf{k}}_b=\cos(\pi/2)$.

Now we consider the case of equal-energy secondary electrons $E_a=E_b$. In this case, the scattering amplitudes T_a,T_b from electrons a and b are of the same order and coincide at $\theta_b=90°$ due to symmetry [Fig. 2(a)]. That means in this case that the projectile ionizes the two target electrons simultaneously. From Eqs. (3)–(5) it is evident, however, that only single-particle perturbation operators are present and the projectile does not directly interact with the center-of-mass of the two electrons. Thus, double ionization must occur via a coherent superposition of the amplitudes T_a and T_b [Fig. 2(a)]. The cross section $\sigma_{a,b}(\theta_b)$ [Fig. 2(a)] exhibits a minimum at $\theta_b\approx72°$. This minimum is due to interference of T_a and T_b and incidentally coincides with the minimum of the average momentum transferred to the nucleus k_{av} at $\theta_b\approx72°$ [Fig. 2(b)]. This could be inferred from the structure of the incoherent contributions of T_a and T_b, which reveal broad maxima around $\theta_b=94°$ and $\theta_b=84°$, respectively. At $\theta_b=0$ the cross section vanishes due the electron-electron repulsion in the final state. Obviously, in the case of Figs. 2(a)–(c) the cross section is very sensitive to the weighting of the coherent amplitudes T_a and T_b, which are determined by the wave functions $\psi^-_{\mathbf{k}_a,\mathbf{k}_b}(\mathbf{r}_a,\mathbf{r}_b)$ and $\varphi(\mathbf{r}_a,\mathbf{r}_b)$. Therefore, the scattering amplitude from the nucleus T_T, which is mainly due to a poor description of the three-body state, strongly affects the cross section because it considerably alters the interference behavior [Fig. 2(c)]. Therefore, orthogonalized and nonorthogonalized final-state wave functions yield in this case quite different results. The experimental finding is qualitatively reproduced by the orthogonalized

form that seems to better fit the experimental data.

The intermediate situation between the cases displayed in Fig. 1(a) and Fig. 2(c) is shown in Fig. 3. The agreement with the data is satisfactory. From the above arguments it is comprehensible that the term T_T does not severely affect the cross section as in Fig. 2(c). The ionization amplitude T_b provides the major contribution to T_{fi} in the vicinity of the maximum. This leads to the interpretation as in Figs. 1(a)–(b). The scattering term T_a, although smaller than T_b (i.e. $|T_b|>|T_a|$), still considerably interferes with T_b.

IV. ASYMMETRY PARAMETERS FOR $(e,3e-1e)$ REACTIONS

In the preceding section it was shown how information on the double-ionization process can be extracted from $\sigma_{a,b}$. However, the link to DPI reactions through the optical limit Eq. (7) is lost after integrating over $\mathbf{q}$. To compare with well studied DPI data and to analyze partial waves contributing to the cross section, it is, therefore, appropriate to fix $\mathbf{q}$ and measure the angular distribution of one secondary electron, i.e.,

$$\sigma_{\mathbf{q},a} := \frac{d^6\sigma}{d\Omega_a d\Omega_0 dE_a dE_0} = \int \frac{d^8\sigma}{d\Omega_a d\Omega_b d\Omega_0 dE_a dE_0} d\Omega_b . \tag{15}$$

Hereafter, all angles are measured with respect to $\hat{\mathbf{q}}$, which defines the z axis. The cross section $\sigma_{\mathbf{q},a}$ is proportional to the cross sections $d^6\sigma/(d\Omega_a d\Omega_0 dE_a dE_b)$ and $d^6\sigma/(d^3\mathbf{q}\,d\Omega_a dE_a)$. The latter one reveals the connection to DPI measurements with linear polarized light, where only one photoelectron is resolved in energy and angle $d^3\sigma^{\mathrm{DPI}}/(d\Omega_a dE_a)$, the so-called asymmetry-parameter experiments [6,26–28].

Due to the cylindrical symmetry of $\sigma_{\mathbf{q},a}(\Omega_a)$ with respect to $\mathbf{q}$ the cross section $\sigma_{\mathbf{q},a}$ [Eq. (15)] can be parametrized in the form [29]

$$\frac{d^6\sigma}{d\Omega_a d\Omega_0 dE_a dE_0} = 4\pi \sum_{\ell=0}^{\infty} B_\ell P_\ell(\hat{\mathbf{q}}\cdot\hat{\mathbf{k}}_a), \tag{16}$$

where $B_\ell(\mathbf{q},E_a)$ are angle-independent coefficients and $P_\ell(\hat{\mathbf{q}}\cdot\hat{\mathbf{k}}_a)$ are Legendre polynomials. The coefficient $B_0(\mathbf{q},E_a)$ is related to integrated cross sections. This follows from the relations

$$\frac{d^4\sigma}{d\Omega_0 dE_a dE_0} = 4\pi \sum_{\ell=0}^{\infty} B_\ell \frac{4\pi}{2\ell+1} \times \sum_{m=-\ell}^{\ell} \int d\Omega_a\, Y_{\ell m}(\hat{\mathbf{k}}_a) Y^*_{\ell m}(\hat{\mathbf{q}}) = 16\pi^2 \sum_{\ell=0}^{\infty} B_\ell \sum_{m=-\ell}^{\ell} \frac{1}{2\ell+1} \delta_{\ell 0}\delta_{m0}, \tag{17}$$

which lead to

$$B_0(\mathbf{q},E_a) = \frac{1}{16\pi^2} \frac{d^4\sigma}{d\Omega_0 dE_a dE_0}. \tag{18}$$

Thus, it is advantageous to renormalize the coefficients B_ℓ to B_0 to end up with dimensionless generalized asymmetry parameters $B^s_\ell = B_\ell/B_0$:

$$\sigma_{\mathbf{q},a} = \frac{1}{4\pi} \frac{d^4\sigma}{d\Omega_0 dE_a dE_0} \sum_{\ell=1}^{\infty} [1 + B^s_\ell P_\ell(\cos\theta_a)]. \tag{19}$$

The equivalent parametrization of $d^3\sigma^{\mathrm{DPI}}/(d\Omega_a dE_a)$ is limited to two terms due to the definite angular momentum imparted to the system by the photon and to the polarization vector entering bilinearly in the cross section, i.e., the polarization vector actually defines an axis rather than a direction,

$$\frac{d^3\sigma^{\mathrm{DPI}}}{d\Omega_a dE_a} = 4\pi \sum_{\ell=0}^{\infty} B^{\mathrm{DPI}}_\ell P_\ell(\cos\theta_a) = \frac{1}{4\pi} \frac{d\sigma}{dE_a}[1 + \beta P_2(\cos\theta_a)]. \tag{20}$$

Here θ_a refers to the emission angle of the photoelectron with respect to the polarization vector which can be chosen to coincide with $\hat{\mathbf{q}}$. Hence, the angular distributions of photoelectrons are essentially characterized by only one parameter, the *asymmetry parameter* $\beta \in [-1,2]$. Thus, the comparison of the asymmetry parameters B^s_ℓ and β gives direct information on the optical limit. To establish a relation between B_ℓ and B^{DPI}_ℓ we consider a DPI and a $(e,3e)$ reactions leading to the same final state of secondary electrons, i.e., $\mathbf{k}^{\mathrm{DPI}}_a = \mathbf{k}_a$ and $\mathbf{k}^{\mathrm{DPI}}_b = \mathbf{k}_b$, where $\mathbf{k}^{\mathrm{DPI}}_a, \mathbf{k}^{\mathrm{DPI}}_b$ are the momenta of electrons produced in a DPI process. Assuming length formulation the cross section, given by Eq. (20), reads

$$\frac{d^3\sigma^{\mathrm{DPI}}}{d\Omega_a dE_a} = 4\pi^2 \alpha\omega k_a k_b \int |\langle \psi^-_{\mathbf{k}_a,\mathbf{k}_b}(\mathbf{r}_a,\mathbf{r}_b)|\hat{\mathbf{q}}(\mathbf{r}_a+\mathbf{r}_b)|\varphi(\mathbf{r}_a,\mathbf{r}_b)\rangle|^2 d\Omega_b, \tag{21}$$

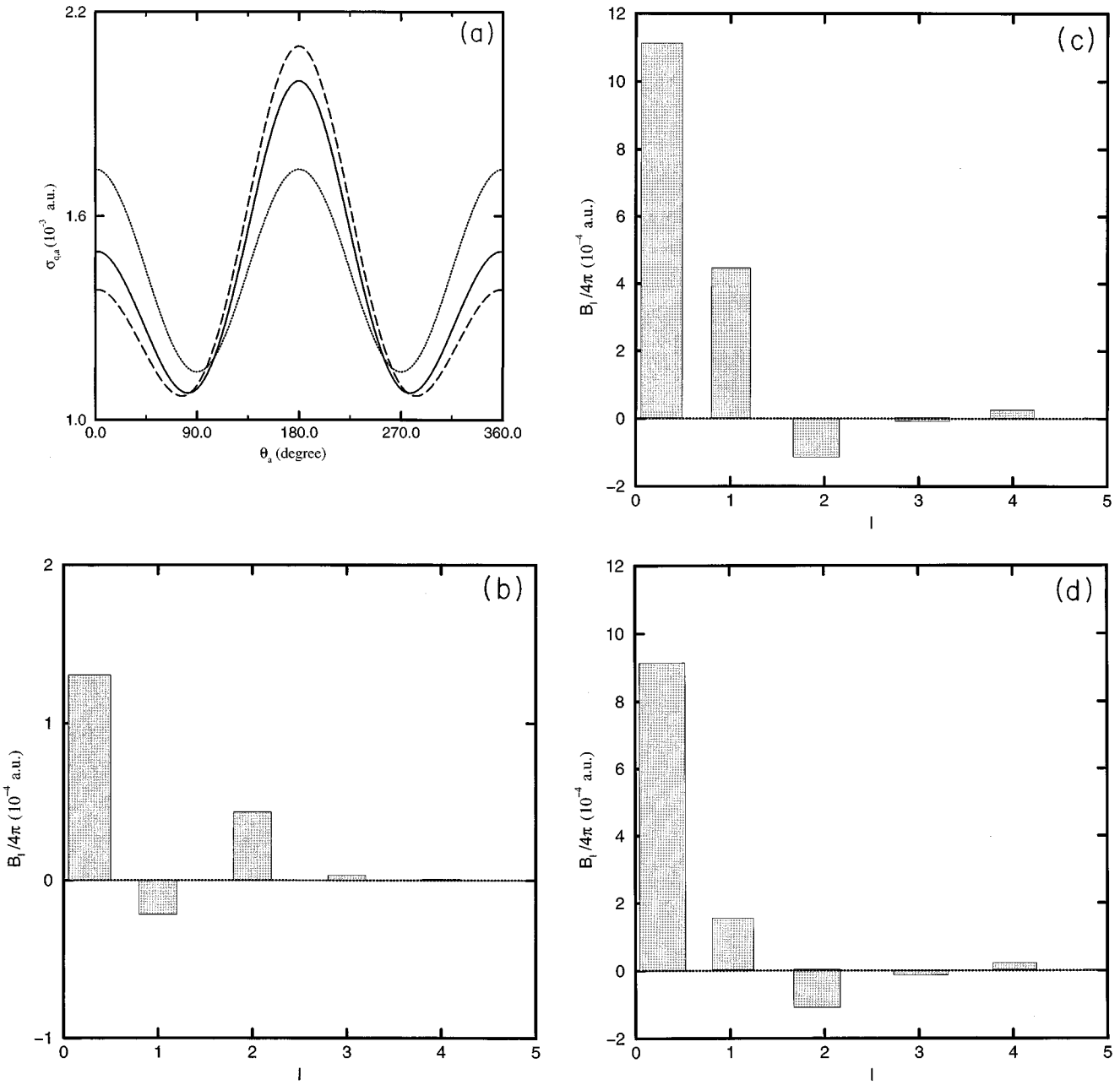

FIG. 4. (a) Cross section $\sigma_{\mathbf{q},a}(\theta_a)$, as defined by Eq. (15), as a function of $\theta_a=\cos^{-1}\hat{\mathbf{q}}\cdot\hat{\mathbf{k}}_a$. The incident energy is $E_i=8$ keV. The scattered projectile is detected under an angle of 1° with respect to $\mathbf{k}_i$ and with energy $E_0=7.8$ keV. The momentum transfer is then $q=0.509$ a.u. The secondary electron is detected with energy $E_a=0.01$ eV. Results of orthogonalized (dashed curve) and nonorthogonalized (solid curve) wave functions are shown. The dotted curve displays the corresponding DPI cross section, as given by Eq. (20), but with coefficients $\bar{B}_\ell^{\mathrm{DPI}}$ [see Eq. (22)]. The DPI asymmetry parameter is equal to $\beta=0.297\,28$. (b) The asymmetry coefficient B_ℓ as a function of ℓ [compare Eq. (16)]. The collision geometry is chosen as in (a). For DPI we obtain $B_0^{\mathrm{DPI}}/4\pi=1.34\times10^{-3}$, $B_2^{\mathrm{DPI}}/4\pi=0.3984\times10^{-3}$ (note $\beta=B_2^{\mathrm{DPI}}/B_0^{\mathrm{DPI}}=0.297$). (c) The asymmetry coefficient B_ℓ as function of ℓ for the same collision arrangement as in (a); however, the secondary electrons are emitted with equal energies. An orthogonalized wave function is used to describe the final state of the two secondary electrons. $B_0^{\mathrm{DPI}}/4\pi=9.04\times10^{-4}$, $B_2^{\mathrm{DPI}}/4\pi=-0.49\times10^{-4}$. (d) The same as (c) but the final-state wave function is not orthogonal to the initial bound state of He($^1S^e$).

where ω is the light frequency and α is the fine-structure constant. According to Eqs. (7,1,21) the parameters B_ℓ tend to scaled DPI-expansion coefficients $\bar{B}_\ell^{\mathrm{DPI}}$ in the optical limit, where

$$\bar{B}_\ell^{\mathrm{DPI}}=(2\pi)^4\frac{4k_0}{k_i q^2\alpha\omega}B_\ell^{\mathrm{DPI}}. \tag{22}$$

A typical example is depicted in Fig. 4(a). The momentum transfer is moderate and the optical limit is approached. Consequently, orthogonalized and nonorthogonalized final-state wave functions yield almost the same $(e,3e-1e)$ results, as predicted above. All cross sections are symmetric with respect to $\theta_a=\pi$. In addition, $d^3\sigma^{\mathrm{DPI}}/(d\Omega_a dE_a)$ is symmetric to the line perpendicular to the polarization vector. The

latter symmetry is destroyed in the case of the $(e,3e-1e)$ reaction since, unlike the situation in DPI where the polarization vector defines an axis leading to the reflection symmetry at $\theta_a=90°$ and 270°, $\mathbf{q}$ fixes a direction. This fact is reflected by B_1^{DPI} being identically zero, whereas B_1 [Eq. (15)] is finite [Fig. 4(b)]. Apart from this difference B_ℓ and B_ℓ^{DPI}, $\ell\neq 1$ are almost equal, as can be seen in Fig. 4(b). Thus, the asymmetry parameter $B_1^s=B_1/B_0$ can be interpreted as indicator for the ''memory'' of the ionized electron to the initial incident direction. The parameter B_2^s is directly linked to β. To understand its physical meaning we assume $q\ll 1, B_1^s\ll 1$. If β (and correspondingly B_2^s) vanishes electron a has an isotropic angular distribution that reflects the symmetry of the initial target state, and hence, this electron is emitted by a shake-off process, whereas the other electron is knocked out after a direct encounter with the projectile. This case occurs when $E_b/E_a\ll 1$ [see Figs. 4(a, b)]. Reversal of the roles of the two secondary electrons, i.e., $E_a/E_b\ll 1$, leads to $\beta=2$, which means that electron a is directly ionized by a binary collision with the projectile, and hence, appears predominantly under the direction $\mathbf{q}$. In these two cases the ejected electrons are weakly correlated. However, a negative value of β indicates that electron a is emitted under a direction considerably different from $\mathbf{q}$ (perpendicular to $\mathbf{q}$ for $\beta=-1$). In this case the double ionization occurs via electronic correlations. That stronger electronic correlations lead to a negative value of B_2 is evident by comparing Fig. 4(a) and Figs. 4(c),(d), where the two target electrons escape with equal energies. However, since the excess energy is relatively high $E_a+E_b=120$ eV the electronic correlation is less prominent when the two electrons are separated in angles. This situation changes drastically for lower excess energies and B_2^s tends to -1. From the preceding we conclude that the asymmetry parameter B_2^s is a measure for the electronic correlations.

As obvious from Eq. (19), the coefficient B_0 determines the absolute value of the cross section. Thus, relative $(e,3e-1e)$ cross sections can be calibrated to DPI data by extrapolating the coefficient B_0 to the quantity $\bar{B}_0^{\mathrm{DPI}}$, as defined by Eq. (22).

To formulate the above heuristically stated argument in a mathematical language we note that with increasing momentum transfer, results with orthogonalized and nonorthogonalized wave functions diverge from each other and an increasing number of partial waves is required to fit the cross sections [24]. This behavior occurs, however, very slowly. More extensive calculations [24] show that for $q<1$ the significant contributions to the series, given by Eq. (19), originate from the first three terms. Thus, assuming $B_\ell^s=0,\forall \ell>2$ the series given by Eq. (19) takes on the form

$$\sigma_{\mathbf{q},a}=\frac{1}{4\pi}\frac{d^4\sigma}{d\Omega_0 dE_a dE_0}[1+\alpha^{e3e}P_1(\cos\theta_a)+\beta^{e3e}P_2(\cos\theta_a)]. \tag{23}$$

In order to express Eqs. (19) and (20) in unified form we introduced in Eq. (23) the redefinition $\alpha^{e3e}\equiv B_1^s$, $\beta^{e3e}\equiv B_2^s$. From Eq. (19) it is clear that, under the assumption $B_\ell^s=0,\forall \ell>2$, only three measurements are necessary to fix the parameters α^{e3e},β^{e3e} and $d^4\sigma/d\Omega_0 dE_a dE_0$ and hence the whole angular distribution $\sigma_{\mathbf{q},a}(\Omega_a)$. The most appropriate geometries under which these measurements can be conducted are, the secondary electron a is detected under a direction perpendicular to $\mathbf{q}$ $[\sigma_\perp:=\sigma_{\mathbf{q},a}(\cos\theta_a=0)]$, parallel to $\mathbf{q}$ $[\sigma_{\uparrow\uparrow}:=\sigma_{\mathbf{q},a}(\cos\theta_a=1)]$, and antiparallel to $\mathbf{q}$ $[\sigma_{\uparrow\downarrow}:=\sigma_{\mathbf{q},a}(\cos\theta_a=-1)]$. From a simple algebraic manipulation the following relations for the asymmetry parameters can be derived:

$$\beta^{e3e}=\frac{2-2x}{1+2x}, \tag{24}$$

$$\alpha^{e3e}=\frac{3}{2}\frac{\sigma_{\uparrow\uparrow}-\sigma_{\uparrow\downarrow}}{\sigma_{\uparrow\uparrow}+\sigma_{\uparrow\downarrow}+2\sigma_\perp}, \tag{25}$$

$$\frac{d^4\sigma}{d\Omega_0 dE_a dE_0}=\frac{4\pi}{3}(\sigma_{\uparrow\uparrow}+\sigma_{\uparrow\downarrow}+2\sigma_\perp), \tag{26}$$

where $x:=2\sigma_\perp/(\sigma_{\uparrow\uparrow}+\sigma_{\uparrow\downarrow})$. Note that Eqs. (24)–(26) are also applicable to DPI processes. From Eq. (25) it is evident that α^{e3e} characterizes the ''memory'' of the ejected electron to the incident direction and thus vanishes identically for a DPI reaction ($\sigma_{\uparrow\downarrow}\equiv\sigma_{\uparrow\uparrow}$). From Eq. (24) it is obvious that the asymmetry parameter β^{e3e} is limited to the interval $\beta^{e3e}\in[-1,2]$. In case the secondary electrons are predominantly ejected along the $\mathbf{q}$ direction ($x\to 0$) β^{e3e} takes on the value $\beta^{e3e}=2$ signifying double ionization by single-binary collision of the projectile with electron a and a shake-off of electron b. If electron a is shaken loose from an S state its angular distribution is isotropic, and hence, $\beta^{e3e}=0$, as can be deduced from Eq. (24). In both cases ($\beta^{e3e}=2,\beta^{e3e}=0$) emitted secondary electrons are weakly correlated. In contrast, if $x\to\infty$ electron a is ejected mainly perpendicular to $\mathbf{q}$, in which case a strong correlation between secondary electrons is acquired, leading to $\beta^{e3e}=-1$, as can be seen from Eq. (24).

A major advantage of expressing $(e,3e-1e)$ cross sections in terms of generalized asymmetry parameters is that it allows a detailed insight into the optical limit. For example from Fig. 4(a) one could conclude that DPI and $(e,3e-1e)$ cross sections are still substantially different and the optical limit is not quite reached yet. However, Fig. 4(b) reveals that the only difference between DPI and $(e,3e-1e)$ reactions in this geometry is the existence of the direction $\mathbf{q}$, i.e., a nonvanishing value of B_1 or α^{e3e} [Eq. (25)]. Apart from that, absolute values of cross sections and the amount of electronic correlations described by B_0 and B_2, respectively, are much the same for DPI and $(e,3e-1e)$ reactions. This means the various respects in which the optical limit is approached can be studied by comparing DPI and $(e,3e-1e)$ asymmetry parameters. This comparison yields far more detailed information on differences between DPI and $(e,3e-1e)$ reactions than the conventional optical formula, given by Eq. (7).

V. CONCLUSIONS

In this work integrated cross sections in $(e,3e)$ reactions have been analyzed. When integrating over the angular distributions of the scattered projectile, two ionization mecha-

nisms are dominant according to the energy sharing of the ionized electrons. It has been explicitly shown that a knock-out collision of a fast ejected electron and a shake-off of the slower one is the dominant mechanism in an asymmetric-energy sharing [3]. For equal-energy sharing the two electrons are ionized simultaneously. In addition, an experimental setup has been proposed that is most suitable to study $(e,3e-1e)$ cross sections in terms of generalized asymmetry parameters. The connection of these asymmetry parameters to their counterparts in a DPI reaction has been worked out. The comparison of DPI with $(e,3e-1e)$ asymmetry parameters allows a detailed insight into the optical limit. Finally, it should be stressed that the analysis of this work is valid only in the range of validity of the Born approximation for the projectile-target interaction.

ACKNOWLEDGMENTS

I would like to thank Professor A. Lahmam-Bennani and his group for stimulating discussions and for many constructive comments on this work. I also would like to thank Hubert Klar, Steve Buckman, and Erich Weigold for helpful comments and suggestions. This work was supported by the Alexander von Humboldt Foundation and the Australian National University under Contract No. V.3-FLF.

[1] A. Lahmam-Bennani, C. Dupŕe, and A. Duguet, Phys. Rev. Lett. **63**, 1582 (1989).
[2] A. Lahmam-Bennani, A. Duguet, A. M. Grisogono, and M. Lecas, J. Phys. B **25**, 2873 (1992).
[3] A. Lahmam-Bennani, J. Phys. B **24**, 2401 (1991).
[4] O. Schwarzkopf, B. Krässing, J. Elmiger, and V. Schmidt, Phys. Rev. Lett. **70**, 3008 (1993).
[5] P. Lablanquie, J. Mazeau, L. Andric, P. Selles, and A. Huetz, Phys. Rev. Lett. **74**, 2192 (1995).
[6] A. Huetz, P. Selles, D. Waymel, and J. Mazeau, J. Phys. B **24**, 1917 (1991).
[7] A. Huetz, P. Lablanquie, L. Andric, P. Selles, and J. Mazeau, J. Phys. B **27**, L13 (1994).
[8] J. Berakdar and H. Klar, J. Phys. B **26**, 4219 (1993).
[9] A. Lahmam-Bennani, H. Ehrhardt, C. Dupŕe, and A. Duguet, J. Phys. B **24**, 3645 (1991).
[10] A. Duguet and A. Lahmam-Bennani, Z. Phys. D **23**, 383 (1992).
[11] B. El Marji, A. Duguet, A. Lahmam-Bennani, M. Lecas, and H. F. Wellenstein, **26**, L733 (1995).
[12] B. Joulakian, C. Dal Cappello, and M. Brauner, J. Phys. B **25**, 2863 (1992).
[13] B. Joulakian and C. Dal Cappello, Phys. Rev. A **47**, 3788 (1993).
[14] C. Dal Cappello and H. Le Rouzo, Phys. Rev. A **43**, 1395 (1991).
[15] R. J. Tweed, J. Phys. B **6**, 270 (1973).
[16] F. Smirnov Yu, A. V. Pavlitchenkov, V. G. Levin, and G. Neudatchin, J. Phys. B **11**, 20 (1978).
[17] J. Berakdar, J. Phys. (France) IV **3**, C6-135 (1993).
[18] H. Bethe, Ann. Phys. (Leipzig) **5**, 325 (1930).
[19] M. Inokuti, Rev. Mod. Phys. **43**, 297 (1971).
[20] M. Inokuti, Y. Itikawa, and J. E. Turner, Rev. Mod. Phys. **50**, 23 (1978).
[21] A. Hylleraas, Z. Phys. D **54**, 347 (1929).
[22] T. A. Carlson and M. O. Krause, Phys. Rev. **140**, 1057 (1965).
[23] T. A. Carlson, Phys. Rev. **156**, 142 (1967).
[24] J. Berakdar (unpublished).
[25] I. E. McCarthy and E. Weigold, Rep. Prog. Phys. **54**, 781 (1991).
[26] R. I. Hall, L. Avaldi, G. Dawber, M. Zubek, K. Ellis, and G. C. King, J. Phys. B **24**, 115 (1991).
[27] R. Wehlitz, F. Heiser, O. Hemmers, B. Langer, A. Menzel, and U. Becker, Phys. Rev. Lett. **67**, 3764 (1991).
[28] F. Maulbetsch and J. S. Briggs, J. Phys. B **26**, 1679 (1993).
[29] H. Klar and M. Fehr, Z. Phys. D **23**, 295 (1992).